IEEE Access
Multidisciplinary ⋮ Rapid Review ⋮ Open Access Journal

Received September 9, 2019, accepted September 29, 2019, date of current version October 17, 2019.

Digital Object Identifier 10.1109/ACCESS.2019.2946057

An LSTM Short-Term Solar Irradiance Forecasting Under Complicated Weather Conditions

YUNJUN YU[1,2], (Member, IEEE), JUNFEI CAO[1], AND JIANYONG ZHU[3], (Member, IEEE)

[1]School of Information Engineering, Nanchang University, Nanchang 330031, China
[2]Institute of Artificial Intelligence, Nanchang University, Nanchang 330031, China
[3]School of Electrical and Electronic Engineering, East China Jiaotong University, Nanchang 330029, China

Corresponding author: Yunjun Yu (yuyunjun@ncu.edu.cn)

This work was supported in part by the National Natural Science Foundation of China under Grant 61563034, and in part by the International S&T Cooperation Program of China under Grant 2014DFG72240.

ABSTRACT Complicated weather conditions lead to intermittent, random and volatility in photovoltaic (PV) systems, which makes PV predictions difficult. A recurrent neural network (RNN) is considered to be an effective tool for time-series data prediction. However, when the weather changes intensely, the long-term sequence of multivariate may cause gradient vanishing (exploding) during the training of RNN, leading the prediction results to local optimum. Long short-term memory (LSTM) network is the deep structure of RNN. Due to its special hidden layer unit structure, it can preserve the trend information contained in the long-term sequence, which is allowed to solve the problems of RNN and improve performance. An LSTM-based approach is applied for short-term predictions in this study based on a timescale that encompasses global horizontal irradiance (GHI) one hour in advance and one day in advance. Inaccurate forecasts usually occur on cloudy days, and the results of ANN and SVR in the literature prove this. To improve prediction accuracy on cloudy days, the clearness-index was introduced as an input data for the LSTM model and to classify the type of weather by k-means during the data processing, where cloudy days are classified as the cloudy and the mixed(partially cloudy). NN models are established to compare the accuracy of different approaches and the cross-regional study is to prove whether the method can be generalizable. From the results of hourly forecast, the R^2 coefficient of LSTM on cloudy days and mixed days is exceeding 0.9, while the R^2 of RNN is only 0.70 and 0.79 in Atlanta and Hawaii. From the results of daily forecast, All R^2 on cloudy days is about 0.85. However, the LSTM is still very effective in improving of RNN and more accurate than other models.

INDEX TERMS LSTM, forecasting short-term solar irradiance, complicated weather, comparative research.

I. INTRODUCTION

Distributed PV systems refer to a power generation application system with decentralized resources, a small installed scale and distributed around the users. The voltage of the connected network is usually lower than 35 kV or lower [1], [2]. It mainly uses PV arrays to directly convert solar energy into electrical energy required for power station systems. The characteristics of low loss and low pollution can effectively alleviate the contradiction between energy and environment, which makes it become an important part of the future energy system [3]. The uncontrollable factors such as climate and seasonality lead to the intermittent, random and volatility of PV power generation [4]. The incorporation of unstable distributed PV systems into the grid will interfere with the smooth operation of the grid [5], [6]. As the proportion of solar energy in power systems has gradually increased [7], [8], PV power prediction technology has become crucial. To scientifically formulate the operating mode and scheduling plan of the power system, it is necessary to predict the output power value of PV power generation in the future. Accurate forecasts can help power administrations and companies personnel adjust and optimize power generation plans promptly, improving utilization and economic efficiency of new energy [9], [10].

Generally, methods of PV prediction mainly focus on PV power or solar irradiance. PV power prediction is achieved by constructing a predictive model that maps historical data to PV output power through a deep analysis of a large amount of historical data, mining the potential rules of data.

The associate editor coordinating the review of this manuscript and approving it for publication was Vincenzo Piuri.

The methods include linear regression [11], k-means clustering[12], ARIMA [13], grey theory [14] and artificial neural network (ANN) [15]. PV power forecasting is supported by massive historical power data, which is not suitable for new power plants that are built soon. Several factors are known to influence PV power generation, including the size and the type of module as well as the installation and arrangement of arrays. Once these electrical characteristics have been optimized, however, subsequent PV power generation will mainly depend on meteorological factors, including the proportion of solar irradiance received on the surface of a module [16]. This means that the effective distribution capacity of a PV system can be attained by predicting the likely amount of solar irradiance it will experience and then calculating output power. The meteorological data required for this method can be easily obtained by local weather stations without the need for on-site collection, so it is widely used in distributed PV systems [17]. PV power prediction methods can also be used to predict solar irradiance by simply changing the input data to historical solar irradiance. The following is an introduction to the related works on PV forecasting methods.

Time-series methods are the most common in the field of PV forecasting. The work of Reikard *et al.* [18] focused on ARIMA, as well as a combination of dynamic integrated forecast (DICast) systems and weather research forecast (WRF) models, which allowed regression coefficients to vary over time can capture a great deal of nonlinear variability. In a direct comparison of meteorological and time series models, the ARIMA is more accurate at short horizons, while the numerical weather prediction model is more accurate as the horizon extends. The numerical weather prediction model performed better on a time scale of more than about 2 hours because it was able to predict changes in clouds and weather.

Models using supervised machine learning (ML), such as random forest (RF) and support vector machine (SVM), are becoming increasingly popular and often show promising accuracy. Benali *et al.* [19] used RF methods to predict global horizontal irradiation (GHI), beam normal irradiation (BNI) and diffusion horizontal irradiation (DHI) for time horizons from h+1 to h+6. The improvement brought by the use of RF compared to ANN and smart persistence (SP) increases with the forecasting horizon. A seasonal study is realized and shows that the forecasting of solar irradiation during spring and autumn is less reliable than during winter and summer. De Leone *et al.* [20] used historical data of solar irradiance, environmental temperature, and past energy production to predict the PV energy production for the next day with an interval of 15 min. The technique used is based on v-SVR, a support vector regression model. The forecasts for energy production obtained with the proposed methodology are very accurate, with the R^2 coefficient exceeding 90%. The quality of the predicted values strongly depends on the goodness of the weather forecast, and the R^2 value decreases if the predictions of irradiance and temperature are not very accurate. Although this method is easy to implement, the SVR algorithm is difficult for large-scale training samples.

As ANN has strong nonlinear fitting capabilities, these approaches can be utilized to map complex relationships of this type and also encapsulate simple learning rules that are easily computer-implemented. It has become a trend in the research of forecasting [21]. Leva *et al.* [22] measured the correlation between weather and PV power and introduced a clearness-index to divide the sky state into clear, cloudy and partially cloudy conditions to guide the supervised learning of the ANN and to classify the prediction results to evaluate. Durrani *et al.* [23] and Alfadda *et al.* [24] established models of multi-layer perceptron (MLP). Forecasting results of the above three all showed that ANN and MLP cannot solve the problem of unstable PV power in cloudy conditions.

Deep learning as an advancement of neural networks, making its structure more complex and deep, enhanced the ability to solve complicated problems. Sun *et al.* [25] employs a specialized convolutional neural network (CNN) model that utilizes both sky images and solar panel output history as input to predict 15-minute ahead solar panel generation. On a full year database, the model achieves 26.2% forecast skill on the sunny test set, and 16.1% forecast skill on the cloudy dataset. An RNN is considered to be an effective tool for time-series data prediction. Yu *et al.* [26] demonstrated in previous work that RNN has better prediction performance than backpropagation NN (BPNN) and radial basis function NN (RBFNN) in sunny, rainy and cloudy days. To improve the prediction accuracy, more variables and longer time series need to be added. However, when dealing with multi-variable long-term sequences, RNN has a gradient exploding (vanishing) problem, which leads to a local optimal result. LSTM is a solution for the above problem due to its special hidden layer design, which allowed the RNN with LSTM units to model both short and long term temporal dependencies in time-series data [27]. LSTM has successful applications in Computer Vision, Speech Recognition and Natural Language Processing [28]–[34]. In the field of power research, such as load forecasting [35] and electricity price forecasting [36], it also shows advantages [36], [37].

According to the above literature, inaccurate forecasts usually occur on cloudy days and the accuracy increases depending on the weather forecast. Therefore, an LSTM-based approach is applied for short-term predictions in this study, using historical meteorology as input instead of weather forecasting. To improve prediction accuracy on cloudy days, the clearness-index was introduced as an input data for the LSTM model and to classify the type of weather by k-means during the data processing, where cloudy days are classified as the cloudy and the mixed(partially cloudy). Since the accuracy decreases when time passes, the timescale of forecasts encompasses GHI one hour in advance and one day in advance, including a mesoscale forecast, to verify the persistence of the LSTM model. ARIMA, SVR, BPNN, CNN and RNN models established as a comparative study facilitates the validation of LSTM models in varying climate/location.

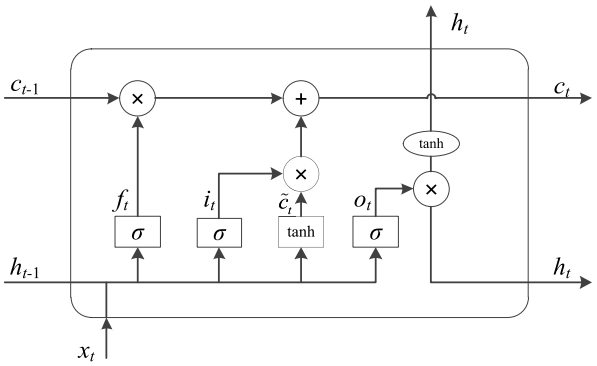

FIGURE 1. LSTM Unit.

II. METHODOLOGY

A. LSTM

Long Short-term Memory Neural Network was proposed by Hochreiter and Schmidhuber in 1997 to avoid long-term dependencies through targeted design. Unlike a single hidden layer of an RNN, LSTM stores information in a control unit outside the normal flow of the RNN, introducing a new state unit C [39]. As shown in Fig. 1, LSTM divides the hidden state of RNN into two parts, memory cells c_t and working memory h_t. The memory cell is responsible for the retention of the sequence features. The memory of the previous sequence is controlled by the forgetting gate f. The working memory h_t is used as the output, and the output gate o controls the portion of the current memory c_t to be written. The input gate i is responsible for controlling the portion of the current state information h_{t-1} and the current input x_t to be written to the memory cells. The above three kinds of gates are not static. The former state information h_{t-1} and the current input x_t are jointly determined by non-linear activation after linear combination. The LSTM architecture can be defined as follows:

$$f_t = \sigma(w_f \times [h_{t-1}, x_t] + b_f) \quad (1)$$
$$i_t = \sigma(w_i \times [h_{t-1}, x_t] + b_i) \quad (2)$$
$$\tilde{c_t} = tanh(w_c \times [h_{t-1}, x_t] + b_c) \quad (3)$$
$$c_t = f_t \times c_{t-1} + i_t \times \tilde{c_t} \quad (4)$$
$$o_t = \sigma(w_o \times [h_{t-1}, x_t] + b_o) \quad (5)$$
$$h_t = o_t \times tanh(c_t) \quad (6)$$

where w_f, w_i, w_c and w_o are weight matrices. b_f, b_i, b_c and b_o are bias vectors. $\tilde{c_t}$ is a new candidate state, which is generated by x_t and h_{t-1} through a tanh layer. $\sigma()$ is the Sigmoid activation function.

B. PERFORMANCE METRICS

Four error metrics were proposed to evaluate the performance of the forecasting model:

Root mean square error (RMSE): measures the difference between the actual values to the forecasting values. A lower RMSE indicates better forecasting result, and is defined:

$$RMSE = \sqrt{\frac{1}{N}\sum_{i=1}^{N}\left(P_f - P_a\right)^2} \quad (7)$$

where N is the amount of observations; P_f is the forecast value; P_a is the actual value.

Mean Absolute Error (MAE): MAE is the average of absolute errors. It can better reflect the accuracy of the forecasting value error, and is defined:

$$MAE = \frac{\sum_{i=1}^{N}\left|P_f - P_a\right|}{N} \quad (8)$$

Mean Absolute Percentage Error (MAPE): MAPE reflects the ratio of error to true value in percentage.

$$MAPE = \frac{1}{N}\sum_{i=1}^{N}\frac{\left|P_f - P_a\right|}{P_a} \times 100\% \quad (9)$$

R-Square (R^2): R-Squared judges whether the predictive model is fitting and reflects the prediction deviates from reality, which ranges from [0, 1]. If $R^2 = 0$, the model fits poorly; if $R^2 = 1$, the model has no errors.

$$R^2 = 1 - \frac{\sum_{i=1}^{N}\left(P_f - P_a\right)^2}{\sum_{i=1}^{N}\left(\bar{P_a} - P_a\right)^2} \quad (10)$$

Among them, RMSE and MAE evaluate the hourly forecast. Problems can occur when calculating the MAPE using the small denominator. MAPE is used to evaluate the daily forecast.

III. DATA PROCESSING

A. DATA COLLECTION

The location determines the climate of the PV station and the distribution and generation of solar irradiance of regions that differ greatly at different latitudes. To explore the scalability of LSTM models, the cross-regional study is necessary. The total amount of daily solar irradiance data from 2013 to 2017 in Atlanta, New York, and Hawaii, USA, was shown in Fig. 2, which was used to plot box plots for observation and filtering of anomalous data. The solar power data is from the National Solar Radiation Data Base (NSRDB) and the collection interval is once per hour. Fig. 2 shows that the median distribution of Atlanta and New York from January to June is gradually increasing, and gradually decreasing from July to December. The median of Hawaii from January to August is 6000 W/m^2, and the number from September to December is 5000 W/m^2. The distribution of GHI in Hawaii is not as seasonal as in Atlanta and New York. The location of each station is shown in Fig. 3.

B. METEOROLOGICAL DATA

In addition to solar irradiance, NSRDB provides us with meteorological data, which are also added as inputs to increase sequence characteristics to improve prediction accuracy. The details of the meteorological data are shown in Table 1. Since LSTM is sensitive to data scales [40],

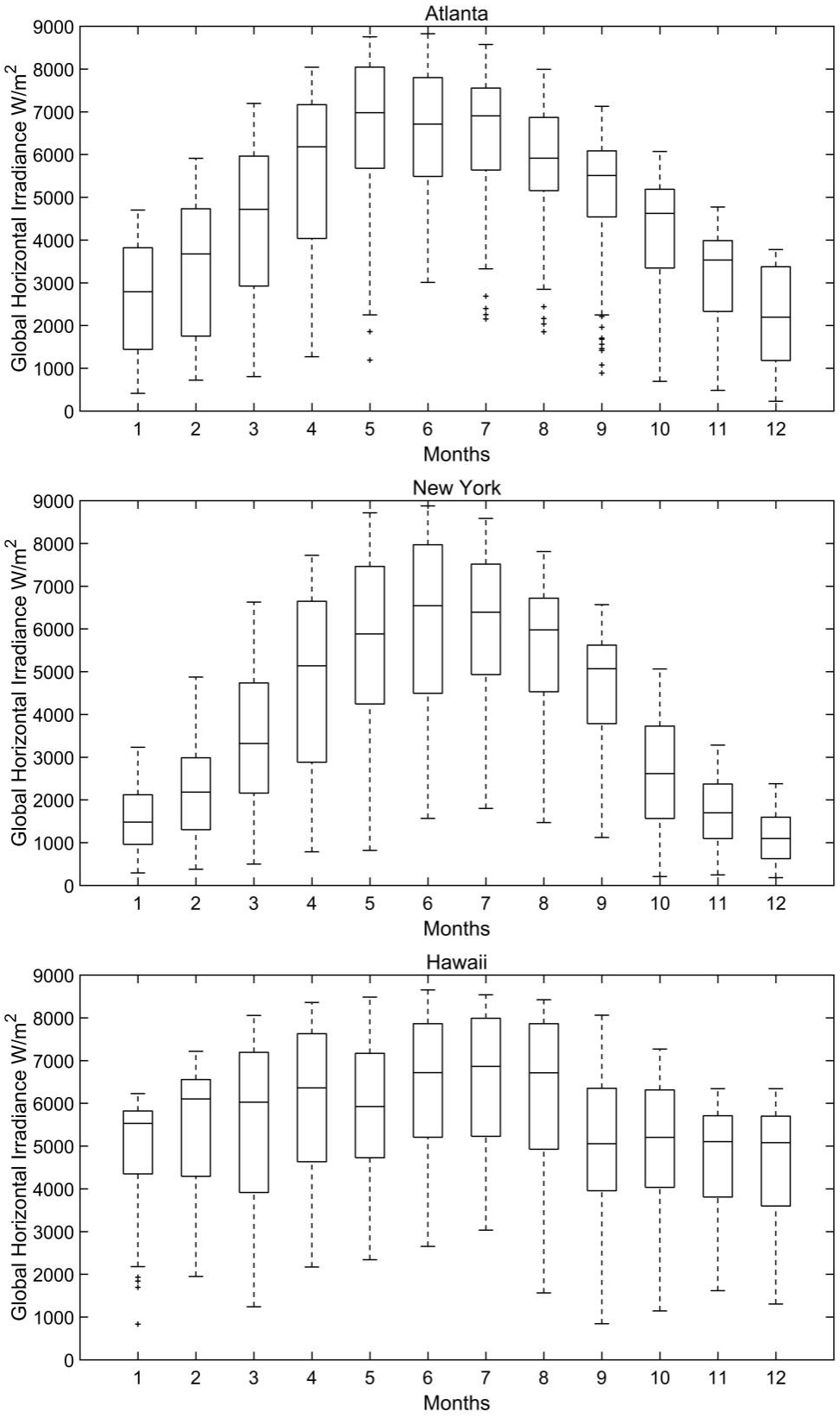

FIGURE 2. Distribution of solar irradiance in each month from 2013 to 2017.

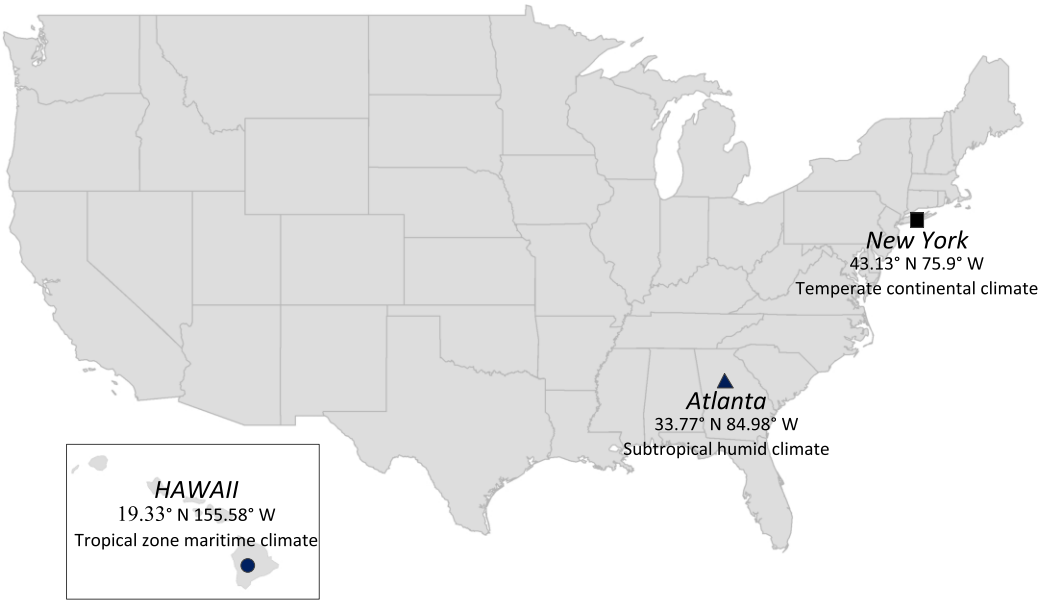

FIGURE 3. Locations and climate types of meteorological station.

TABLE 1. Meteorological data.

	Unit
GHI	W/m^2
Clear-sky GHI	W/m^2
Cloud type	/
Dew point	℃
Temperature	℃
Precipitable water	cm
Relative humidity	%
Solar Zenith Angle	Degree
Wind Speed	m/s
Wind direction	Degrees

TABLE 2. Cloud type.

Cloud type	Level
Clearsky	0
Probably Clear	1
Fog	2
Water	3
Super-Cooled Water	4
Mixed	5
Opaque Ice	6
Cirrus	7
Overlapping	8
Overshooting	9

the data is normalized by Min-Max and transformed to [0, 1], calculated by:

$$x_{norm} = \frac{x - x_{min}}{x_{max} - x_{min}} \tag{11}$$

Among these, the cloud is the main cause of the randomness and volatility of the PV system. According to the NSRDB standard, the cloud is divided into 10 types according to the weather type and cloud level [41]. As shown in Table 2, this is a label encoding. For categorical variables that do not have an ordinal relationship, integer encoding is not sufficient. Using this encoding and allowing the model to assume a natural ordering between categories can lead to poor performance or unexpected results (predictions between categories). In this case, one-hot encoding is applied to integer representations. This is where the integer-encoded variables are removed and a new binary variable is added for each unique integer value. The "1" value is placed in the binary variable of the cloud type, and the value of "0" is placed on the other cloud type.

The clearness-index is also used as an important data to identify the type of weather. In meteorology, the clearness-index is determined by the ratio of GHI to extraterrestrial solar radiation [42]. In the field of PV, more and more researchers have given a broader definition of "clear-sky": in a certain period of time, there is no cloud between the path between the photovoltaic system and the sun, then the sky condition can also be considered It is "clear-sky" and is also called equivalent clear-sky [43]. Therefore, the ratio between GHI and Clear-sky GHI is also used as a description of the amount of cloud. It is defined as:

$$k_t = \frac{GHI}{Clear - skyGHI} \tag{12}$$

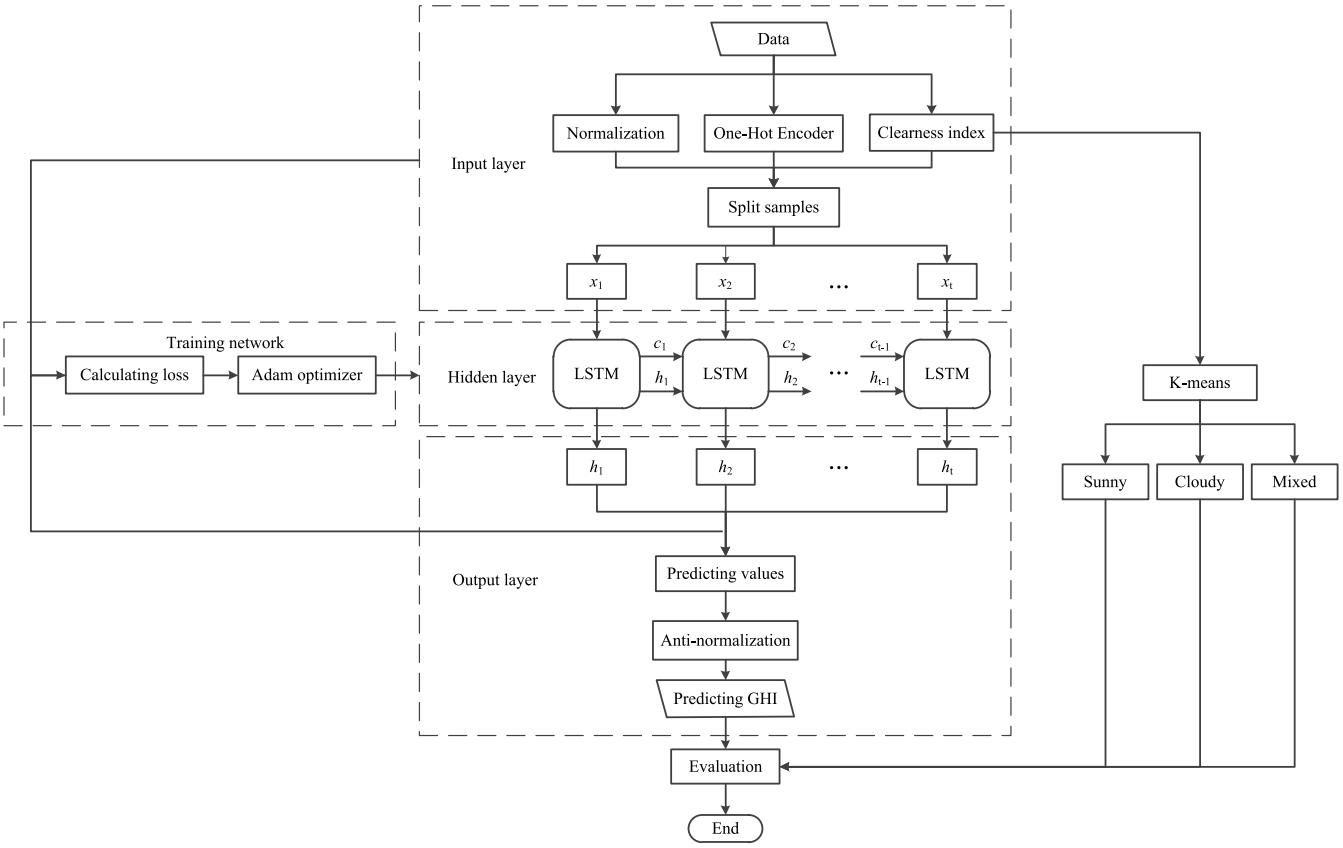

FIGURE 4. LSTM-based GHI prediction framework.

IV. MODEL IMPLEMENTATION

Meteorological data from 2013 to 2016 will be used to train the model, and GHI in 2017 will be used to evaluate the accuracy of the forecast. GHI, meteorological data, and clearness-index for the previous 24 hours will be used as input data for the predictive model. The output data is the total GHI for the next hour and the total GHI for the next 24 hours. Fig. 4 shows the LSTM-based GHI prediction framework. Since this study focuses on the prediction accuracy of the LSTM model in complicated weather, it is necessary to know the distribution of solar radiation in 2017 and classify the weather on the test samples.

The model in this study is a single hidden layer structure. From equations (1) to (3), the selection of the threshold activation function $\sigma(\cdot)$ is the key to the model establishment. Since the ReLU [44] function can alleviate the gradient dispersion problem and the calculation speed is fast, it is chosen as the activation function. Over-fitting is a serious problem in multi-variable multi-parameter deep neural network training [45]. We add the dropout [46] algorithm to the hidden layer, which allows cells (and their connections) to be randomly discarded from the neural network during training. This method can effectively alleviate the over-fitting problem. The output layer calculates the Mean Absolute Error (MAE) as the loss function for the predicted output P_f and the target output P_a. The hidden layer will calculate the gradient calculated by the loss function, and the BP algorithm adjusts the weights in the network [47]. The Adam [48] algorithm is used to generate optimization parameters for each iteration learning until the loss function converges. After the model training is finished, the output layer performs anti-normalization on the result and restores the predicted value to the time-series data corresponding to the input.

The establishment of the LSTM model in the article is based on the keras package. ARIMA, SVR, BPNN, CNN, and RNN forecasting models were also established as comparative experiments, in which BPNN is implemented by MATLAB. The models' configurations are shown in Table 3.

There are as many as thirty-three types of weather defined by the meteorological department [49]. If they are not sorted, the corresponding database of each type requires a large amount of observation data of solar irradiance, and the workload will be very large. Specifically for some very rare weather types, almost no historical data are available. To solve the above problems, we sort types of weather defined by the meteorological department. The K-means was used according to the total GHI of a day and equivalent clearness-index, and the result of classification is as shown in Fig. 5. The weather type is simplified to 3 categories, sunny, cloudy, mixed (partially cloudy), and Table 4 counts the days of the test samples in different types.

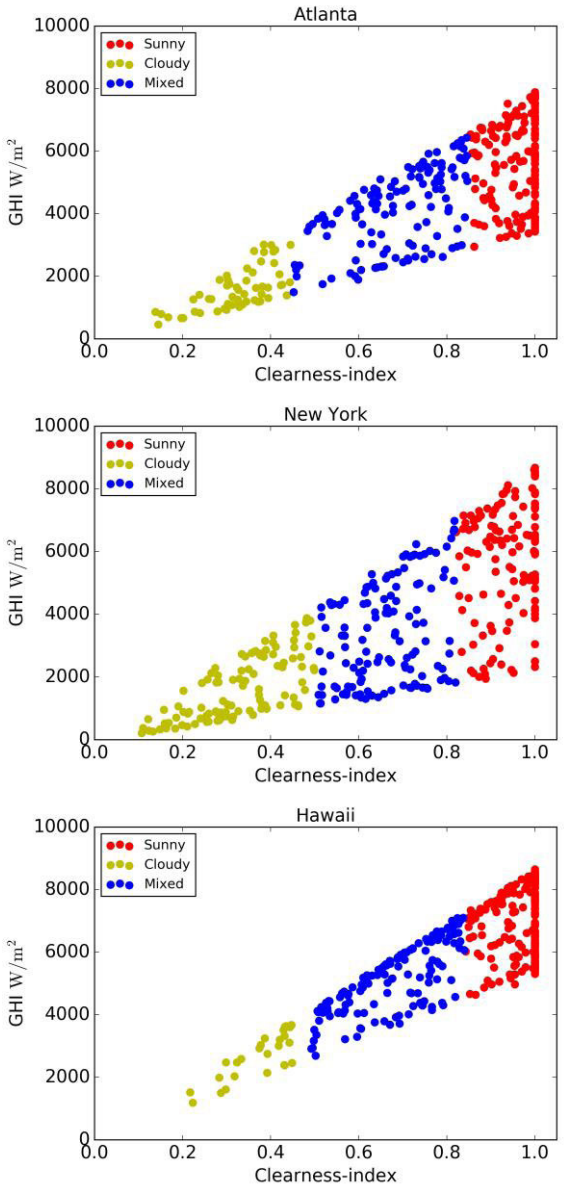

FIGURE 5. Weather classification results of K-means.

V. RESULTS AND DISCUSSION

Fig. 6, Fig. 7, Fig. 8 and Table 5 provide RMSE and MAE for hourly forecasts across regions, ranging from 8:00 to 17:00, as the predicted results at sunset are not shown. Seasons are divided into spring (March to May), summer (June to August), fall (September to November), and winter (January to February, December). In Table 5, All represents the prediction error for all weather conditions.

On sunny days: in Atlanta, the RMSEs for ARIMA, BPNN, RNN and LSTM are 30.44 W/m^2, 31.34 W/m^2, 30.10 W/m^2, 28.65 W/m^2, and MAE is 24.26 W/m^2, 23.07 W/m^2, 26.28 W/m^2, 22.82 W/m^2, which are very close. Their performance differs in the forecasts of New York and Hawaii. From Fig. 7(a), BPNN had problems in prediction on spring, autumn and winter compared with other models. In New York, when LSTM's RMSE and MAE are only

TABLE 3. Models and configuration.

c	Configuration
ARIMA	(p, d, q)=(1, 1, 3), seasonal_order=(1, 1, 1, 12),
SVR	svr_rbf = SVR(kernel='rbf', C=0.8, gamma=0.2)
BPNN	INnum=11，MIDnum=18，OUTnum=1 tansig(Hidden layer)， logsig（Output layer）， GOAL=0.001，SPREAD=0.1
CNN	model.add(Conv1D(filters=32, kernel_size=3, activation='relu', input_shape=(24,11))) model.add(MaxPooling1D(pool_size=2)) model.add(Dropout(0.2)) model.add(Flatten()) model.add(Dense(8, activation='relu')) model.add(Dense(1)) model.compile(loss='mae', optimizer='adam')
RNN	model.add(SimpleRNN (50, input_shape=(24,11) , return_sequences =True))) model.add(Activation('relu')) model.add(Dropout(0.1)) model.add(Dense(1)) model.compile(loss='mae', optimizer='adam')
LSTM	model.add(LSTM(50, input_shape=(24,11) , return_sequences =True))) model.add(Activation('relu')) model.add(Dropout(0.1)) model.add(Dense(1)) model.compile(loss='mae', optimizer='adam')

TABLE 4. Days of the test samples in different types.

	Sunny $k_t > 0.85$	Cloudy $k_t < 0.45$	Mixed $0.45 < k_t < 0.85$
Atlanta	174	53	134
New York	119	85	160
Hawaii	200	26	138

32.05 W/m^2 and 22.56 W/m^2, BPNN and RNN's RMSE are 59.04 W/m^2 and 54.93 W/m^2, MAE is 43.35 W/m^2 and 44.81 W/m^2, which shows significant deviations. R^2

On cloudy days: from Fig. 6(b) and Fig. 7(b), the RNN and LSTM model showed the same excellent predictive performance as LSTM in Atlanta and New York when GHI is low. However, LSTM's RMSE and MAE in Atlanta are 29.18 W/m^2 and 19.11 W/m^2, which is better than RNN's 38.69 W/m^2 and 30.65 W/m^2. From Fig. 8(b), Atlanta's GHI has some volatility on cloudy days, and the results of the predictive model are affected, when the RMSE and MAE of the LSTM are 73.07 W/m^2 and 54.34 W/m^2. Despite the increased error, the predictive performance of LSTM shows advantages compared to other models.

On mixed days: from Table. 5, the MAE and RMSE of all forecasting models multiplies on mixed days compared to sunny and cloudy days, indicating a decrease in prediction accuracy. Fig. 6(c), Fig. 7(c) and Fig. 8(c), LSTM's forecast is closer to the true value, especially at 16:00 in Atlanta on Apr. 17th and 15:00 on Jul. 30th, at 14:00 on Mar. 12th in Hawaii. From Table 5, the RMSE of the LSTM in Atlanta

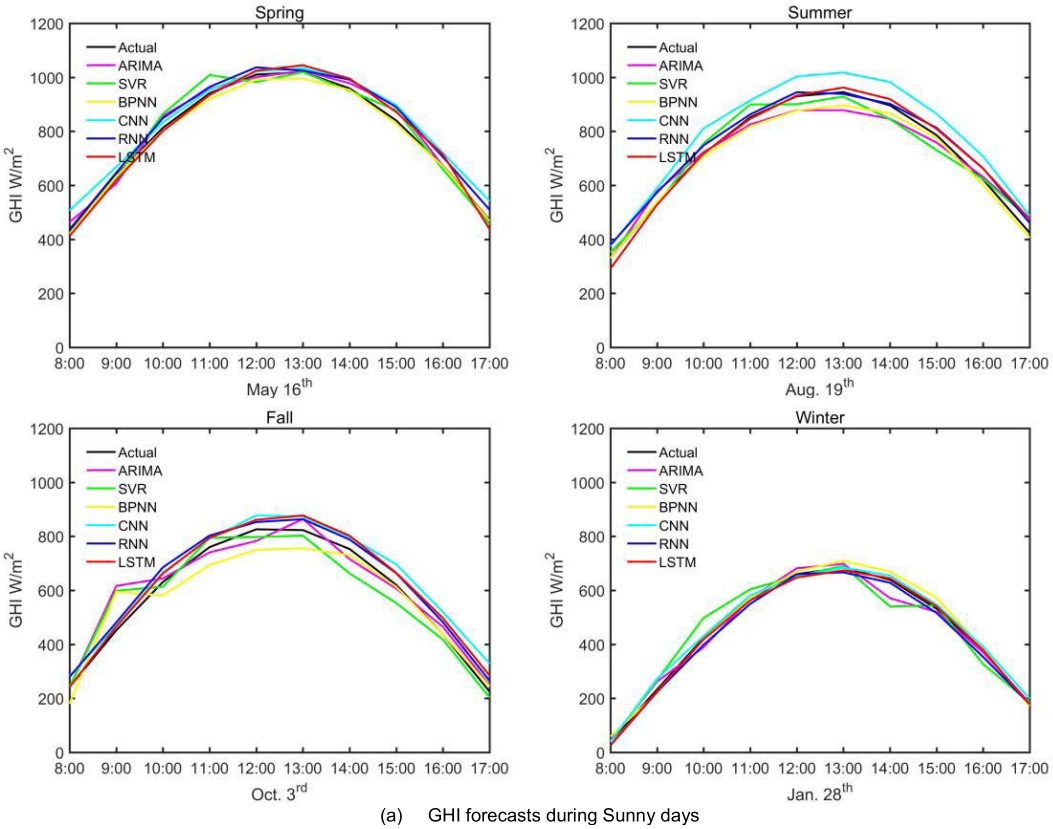

(a) GHI forecasts during Sunny days

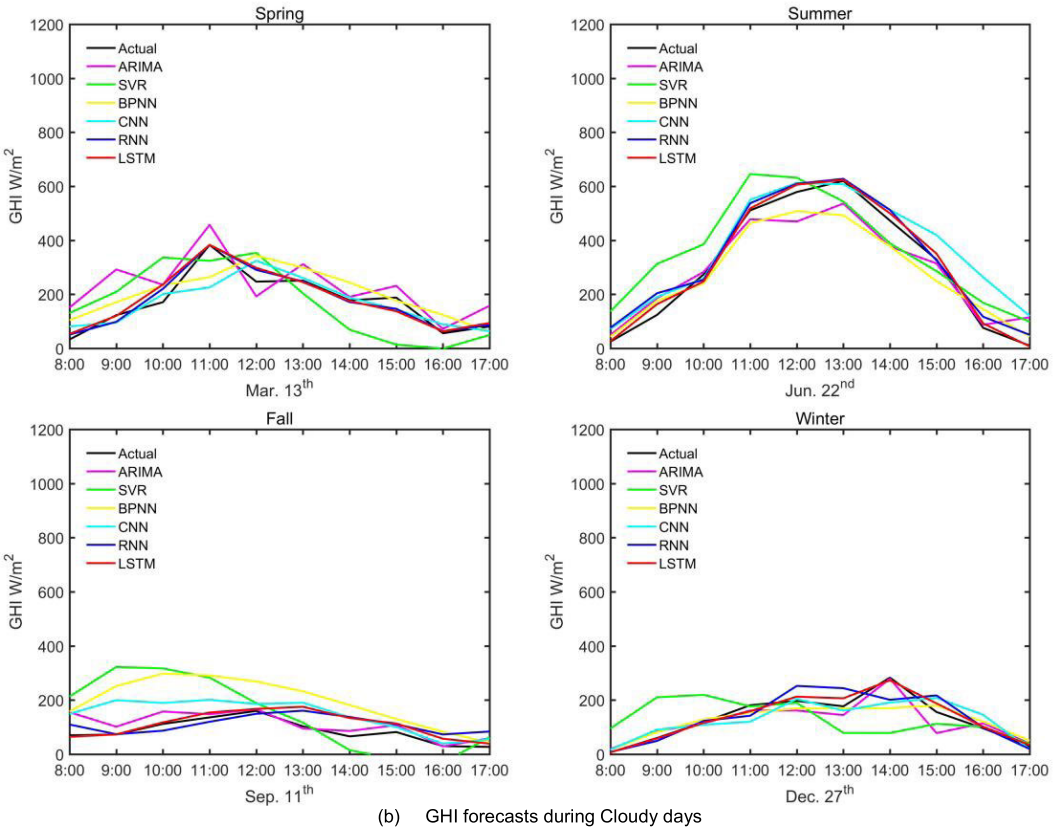

(b) GHI forecasts during Cloudy days

FIGURE 6. Forecasts in Atlanta.

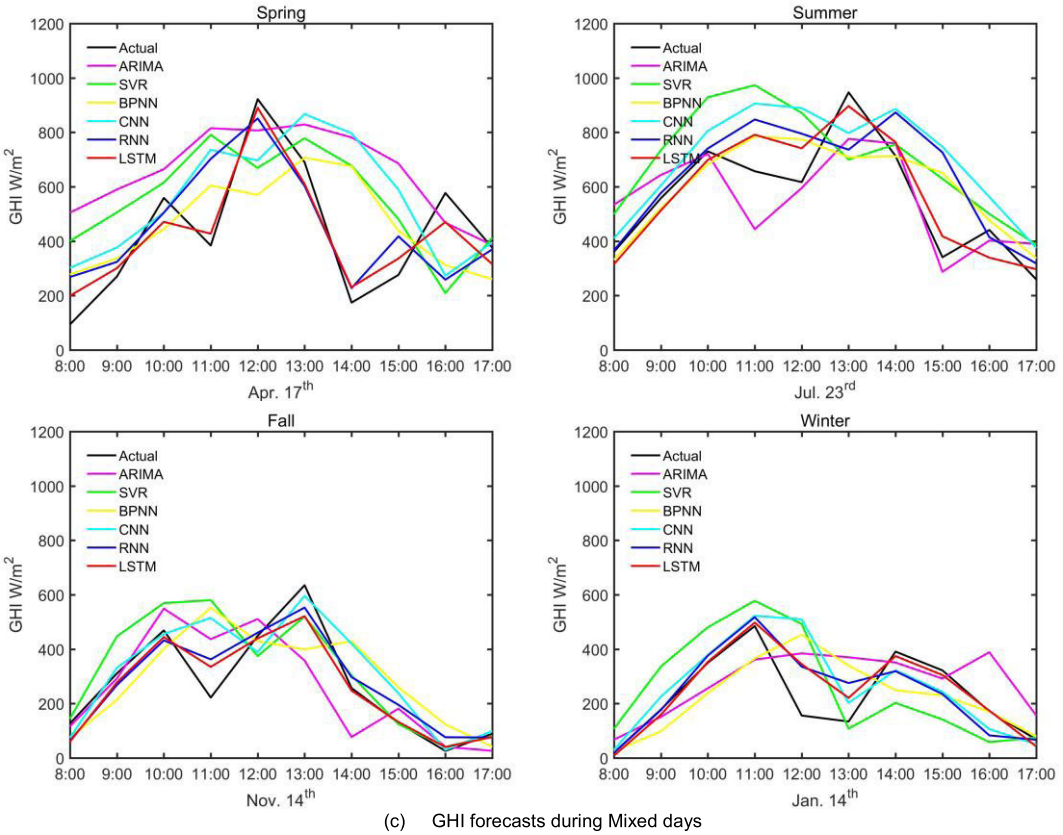

(c) GHI forecasts during Mixed days

FIGURE 6. ***(Continued.)*** **Forecasts in Atlanta.**

is 68.89 W/m^2, whereas the best RMSE between BPNN, CNN and RNN is 130.66 W/m^2, which belongs to RNN. In Hawaii, the advantages of LSTM are even more obvious. The RMSE of LSTM is 86.68 W/m^2, when the RMSE of BPNN, CNN, and RNN are 178.44 W/m^2, 195.92 W/m^2 and 183.29 W/m^2, which almost reduces the error of 100 W/m^2.

Usually, the hourly forecast is to calculate the photovoltaic power by forecasting the solar irradiance at various moments, to adjust the grid configuration and ensure its safe operation. Forecasting the PV power in the next 24 hours is also important for PV power plants to enhance operational efficiency and improve the economy. Table 6 provides the MAPE for daily forecasts across regions. BPNN's best performance occurs in Atlanta on sunny days, but its MAPE is as high as 16.2%, which means it is not suitable for solving this problem. The CNN model performs better on daily forecasts than it does on hourly forecasts, especially in Hawaii, where its MAPE is 12.2% on sunny days and 7.3% on mixed days, which is close to RNN's under the same conditions. RNN's performance is the best among all forecasting models on sunny days with little volatility in weather or GHI. In Atlanta and New York, its MAPE is 5.6% and 7.5%, exceeding the LSTM model. From all days, RNN's MAPE is only 14.5% in New York and less than 10% in Atlanta and New York. The performance gap between RNN and LSTM is revealed on cloudy days and mixed days. RNN has more than 20% of MAPE in all regions and even 27.2% in New York on cloudy days. The MAPE of the LSTM model in Atlanta, New York, and Hawaii on cloudy days is 14.9%, 20.1%, and 18.1, respectively. The LSTM unit is very effective in improving the prediction accuracy of RNN. On mixed days, RNN's MAPE in New York is up to 25.5%, while LSTM's MAPE is 15.3%, which is 10.2% better than RNN. On all days, LSTM's MAPE is the lowest, which is 8.0%, 11.1%, 8.2% in Atlanta, New York, and Hawaii.

As can be seen from the above, the difficulty of daily forecasting is mainly in the prediction of low GHI. Table 7 provides the MAPE for daily forecasts of each month. The results show that LSTM has the vast majority of best predictive performance. We also observed that the MAPE of the LSTM model is up to 20% in New York from January to March and October to December. This result is consistent with the GHI distribution provided in Fig. 3, with low GHI during these times. Despite this, LSTM's annual MAPE is 11.1% in New York, which still has higher prediction accuracy and better performance than other predictive models.

Table 5 and Table 6 also provide the R^2 of the hourly and daily forecasting under different weather conditions. Although ARIMA and SVR's R^2 is about 0.9 in New York,

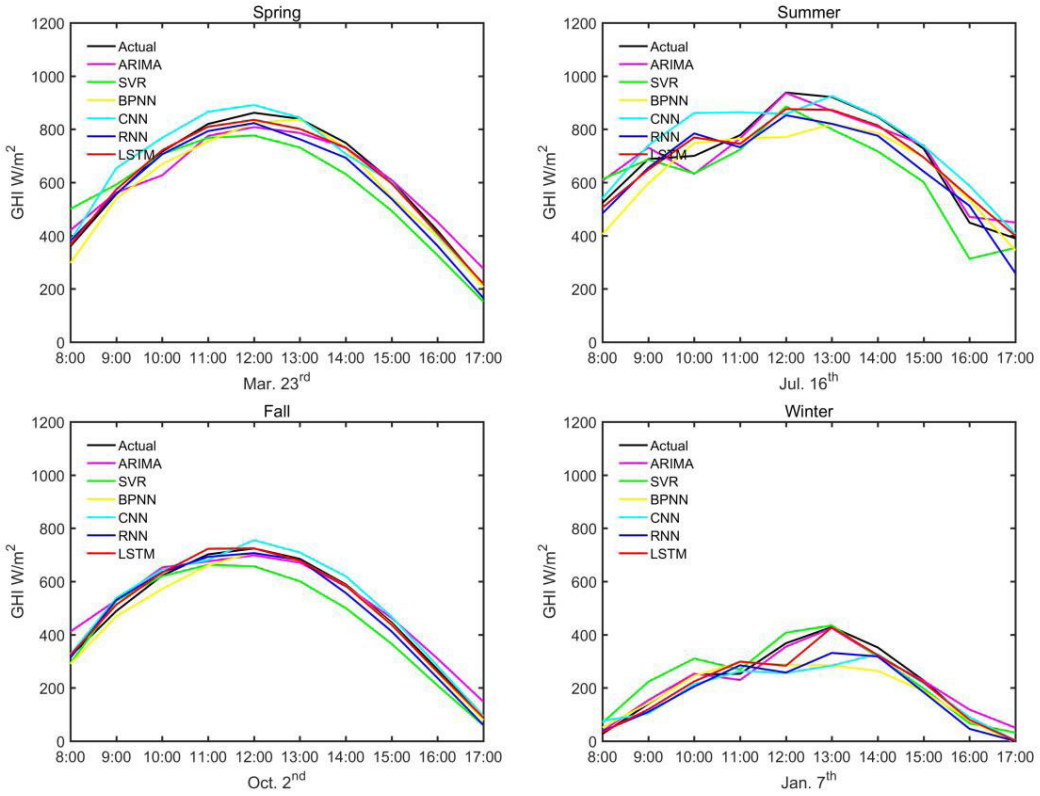

(a) GHI forecasts during Sunny days

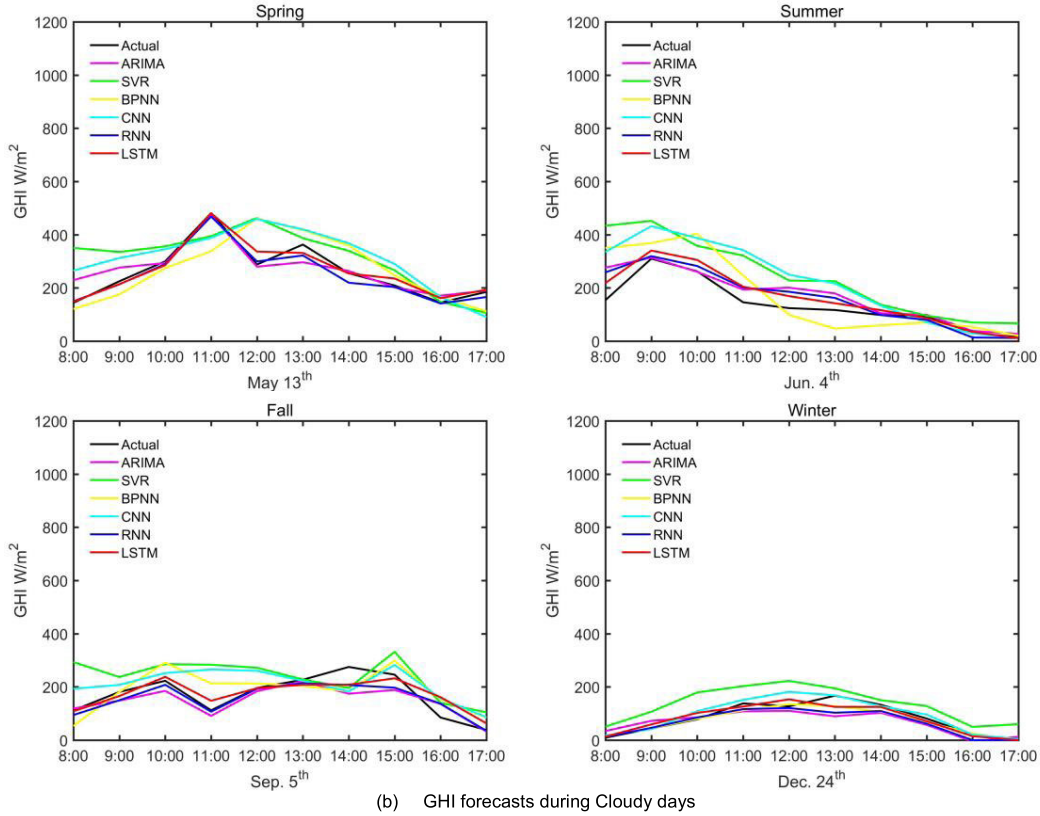

(b) GHI forecasts during Cloudy days

FIGURE 7. Forecasts in New York.

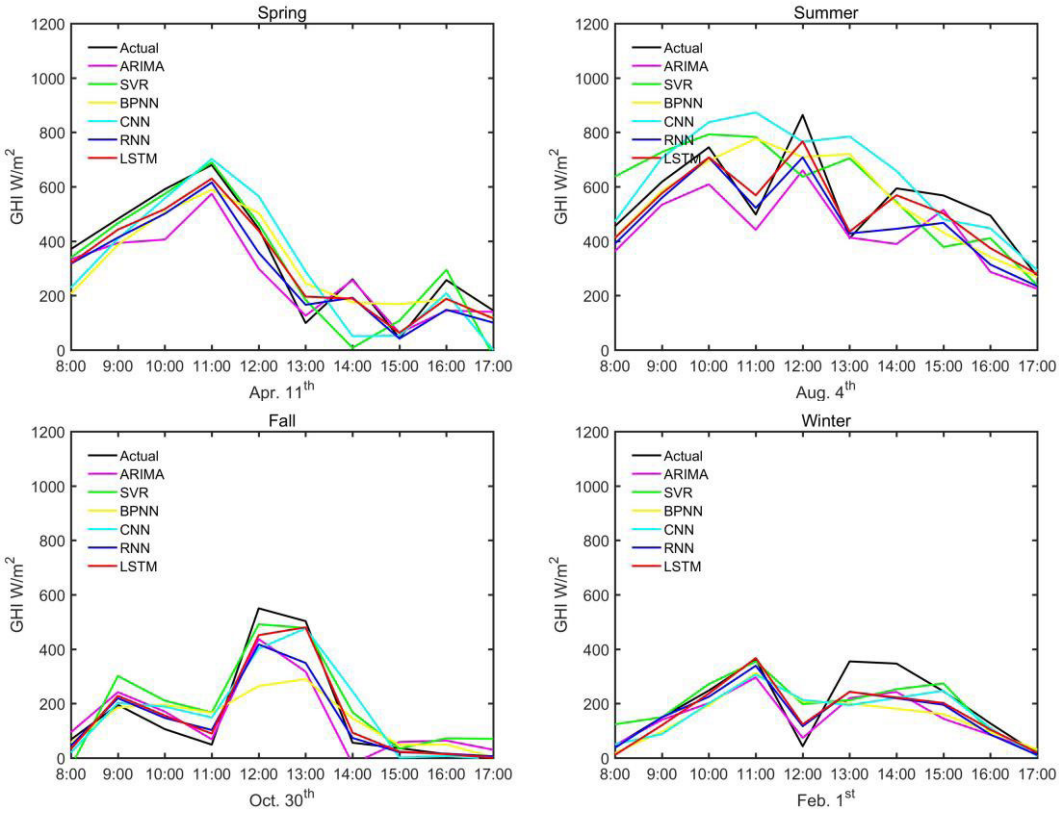

(c) GHI forecasts during Mixed days

FIGURE 7. ***(Continued.)*** **Forecasts in New York.**

TABLE 5. **Evaluation of hourly forecast for chosen locations.**

Location	Model	RMSE (W/m^2)				MAE (W/m^2)				R^2			
		Sunny	Cloudy	Mixed	All	Sunny	Cloudy	Mixed	All	Sunny	Cloudy	Mixed	All
Atlanta	ARIMA	30.44	58.06	166.88	110.78	24.26	53.56	122.639	71.48	0.97	0.86	0.57	0.86
	SVR	35.14	69.49	172.53	116.45	23.33	61.62	132.58	75.84	0.97	0.78	0.49	0.84
	BPNN	31.34	80.19	174.91	112.56	23.07	65.01	134.44	74.17	0.98	0.73	0.45	0.84
	CNN	52.55	65.32	194.64	122.36	44.00	50.50	139.47	77.99	0.96	0.72	0.32	0.82
	RNN	30.10	38.69	130.66	80.57	26.28	30.65	90.55	49.83	**0.99**	0.94	0.70	0.92
	LSTM	**28.65**	**27.18**	**68.89**	**45.84**	**22.82**	**19.11**	**53.65**	**31.86**	**0.99**	**0.97**	**0.92**	**0.97**
New York	ARIMA	42.27	42.66	96.37	65.56	34.23	30.66	74.37	46.58	0.97	0.83	0.83	0.93
	SVR	53.87	61.49	117.38	79.23	42.49	62.36	88.064	57.64	0.96	0.45	0.74	0.90
	BPNN	59.04	69.89	123.10	88.55	43.35	51.11	95.59	63.35	0.95	0.55	0.72	0.88
	CNN	56.15	83.75	124.95	92.70	38.70	63.46	89.01	63.72	0.95	0.35	0.71	0.87
	RNN	54.93	32.49	77.08	57.77	44.81	22.85	60.24	42.64	0.96	0.90	0.89	0.93
	LSTM	**32.05**	**29.59**	**56.86**	**41.37**	**22.56**	**22.03**	**45.97**	**30.19**	**0.99**	**0.92**	**0.94**	**0.97**
Hawaii	ARIMA	35.29	121.49	174.35	133.71	26.26	94.86	139.67	90.50	0.98	0.57	0.60	0.80
	SVR	48.01.	155.22	176.06	144.43	48.65	108.71	149.29	96.25	0.95	0.31	0.48	0.75
	BPNN	80.40	123.49	178.44	133.61	60.13	86.76	132.96	93.29	0.91	0.56	0.52	0.78
	CNN	42.91	159.14	195.92	147.82	35.24	109.42	146.48	97.04	0.97	0.26	0.42	0.74
	RNN	29.90	108.17	183.29	124.09	21.17	83.66	125.08	77.30	0.98	0.66	0.79	0.81
	LSTM	**22.13**	**73.07**	**86.68**	**66.69**	**18.72**	**54.34**	**65.07**	**46.04**	**0.99**	**0.91**	**0.90**	**0.95**

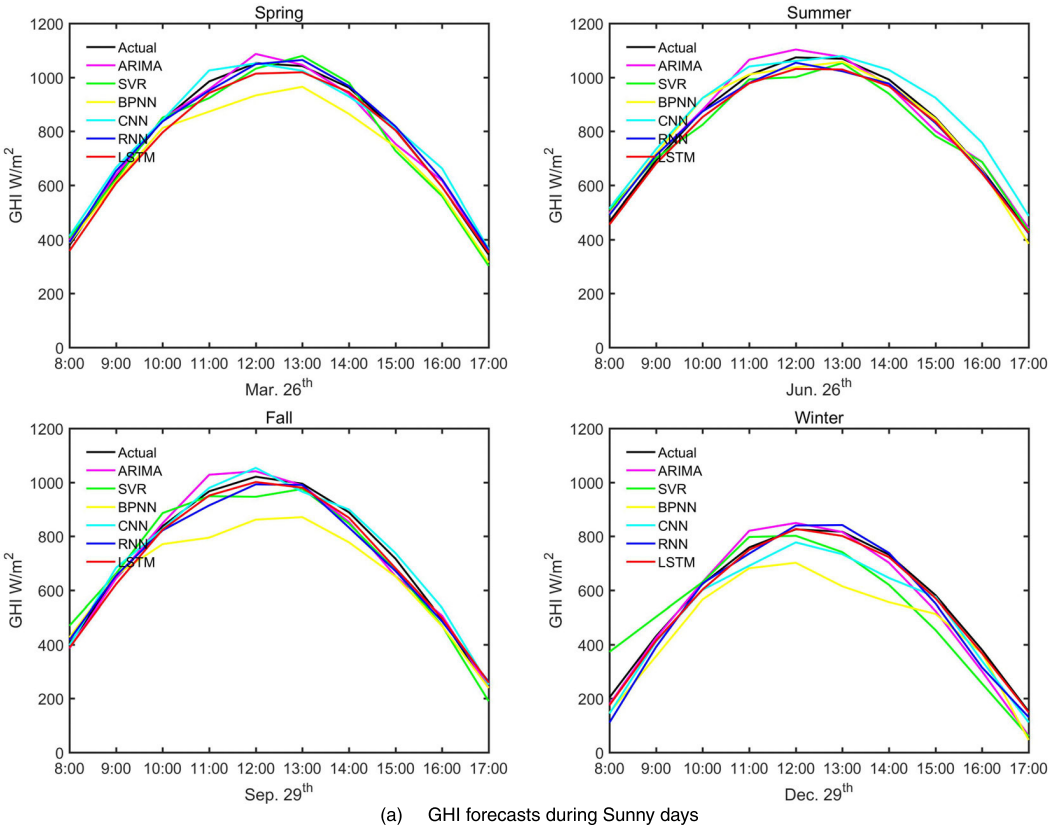

(a) GHI forecasts during Sunny days

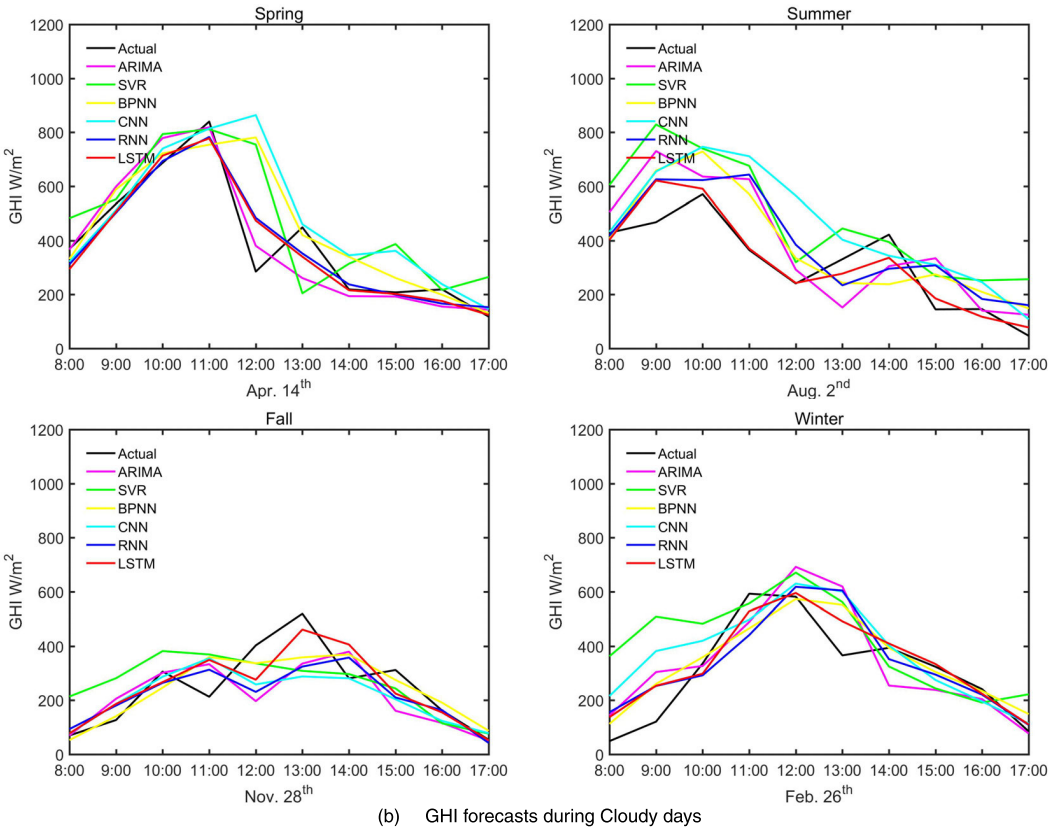

(b) GHI forecasts during Cloudy days

FIGURE 8. Forecasts in Hawaii.

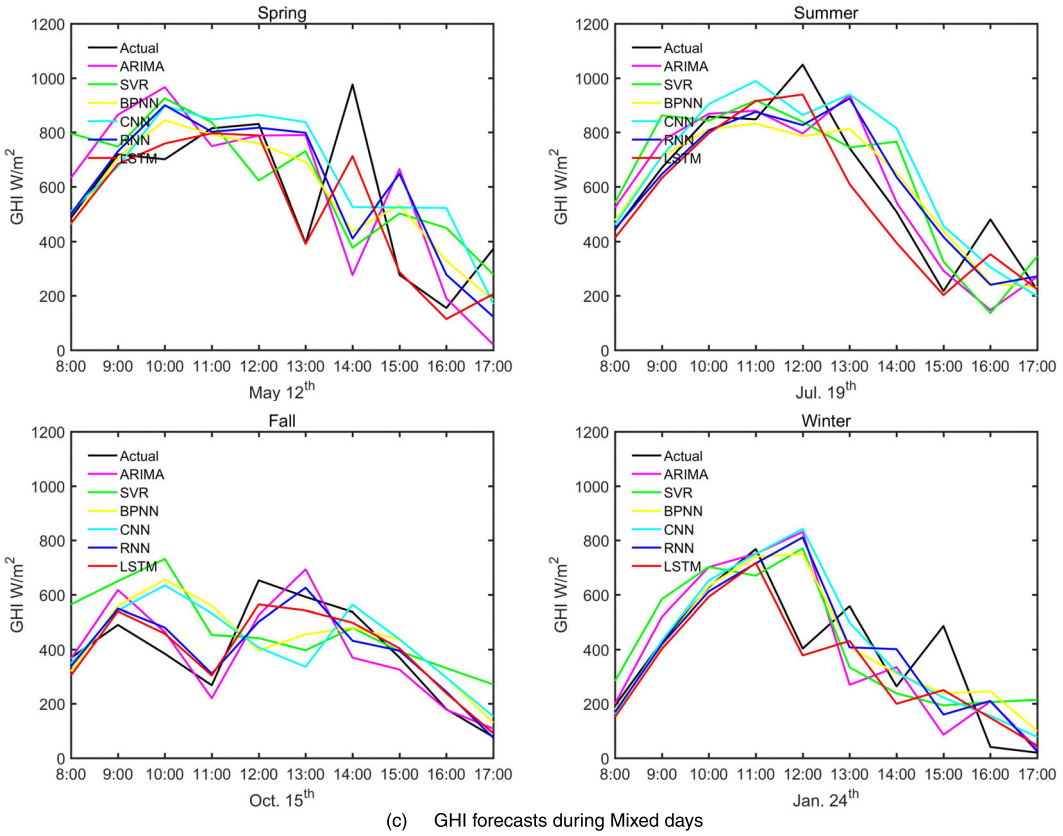

(c) GHI forecasts during Mixed days

FIGURE 8. ***(Continued.)*** **Forecasts in Hawaii.**

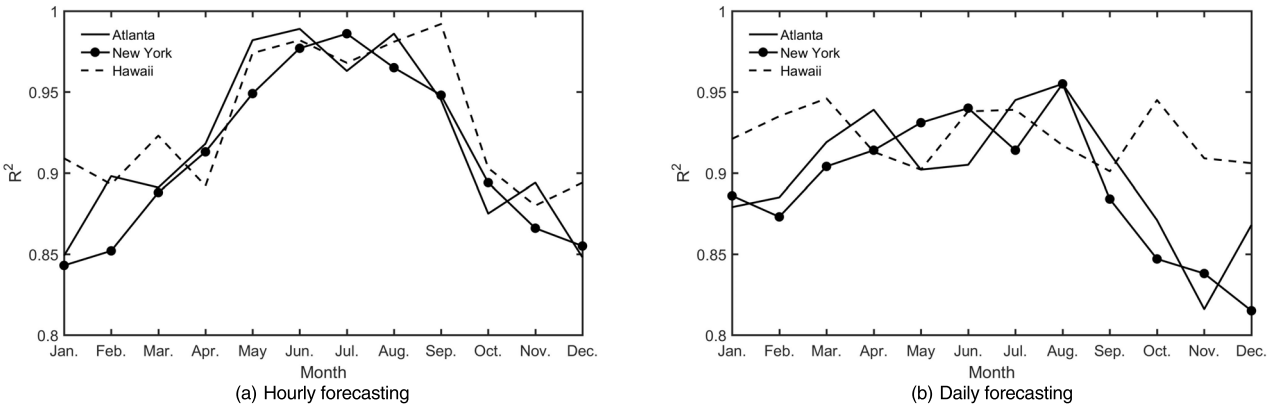

(a) Hourly forecasting (b) Daily forecasting

FIGURE 9. R^2 **of LSTM model per month.**

they are not good at dealing with daily forecasts. In most instances, their R^2 is below 0.8, especially in Hawaii on cloudy days, their R^2 is only 0.53 and 0.54. The R^2 coefficient of LSTM on cloudy days and mixed days is exceeding 0.9, especially, the R^2 of hourly forecasting on sunny days reaches 0.99, which reflects the LSTM model is fitting well. On mixed days, the R^2 of RNN is only 0.70 and 0.79 in Atlanta and Hawaii, which further proves the improvement. Significantly, all R^2 of the daily forecasting on cloudy days is about 0.8. Although these values are below average, the LSTM model still has better predictive performance than other models. The R^2 of LSTM per month is shown in Fig. 9. In Hawaii, the R^2 of LSTM is about 0.9. However, the high value of R^2 in Atlanta and New York is concentrated between April and September, referring to Fig. 3, which is exactly when the daily GHI value is high. LSTM still has the potential to improve predictive performance when GHI is low.

TABLE 6. Evaluation of daily forecast for chosen locations.

Location	Model	MAPE%				R^2			
		Sunny	Cloudy	Mixed	All	Sunny	Cloudy	Mixed	All
Atlanta	ARIMA	10.9	22.9	12.5	12.9	0.79	0.70	0.83	0.87
	SVR	11.6	23.8	17.3	14.8	0.77	0.70	0.72	0.83
	BPNN	16.2	42.1	19.7	21.0	0.76	0.34	0.54	0.59
	CNN	10.4	29.6	16.9	12.5	0.81	0.68	0.80	0.85
	RNN	**5.6**	19.6	7.1	9.4	0.91	0.72	0.93	0.91
	LSTM	7.3	**14.9**	**6.8**	**8.0**	**0.93**	**0.86**	**0.94**	**0.92**
New York	ARIMA	8.5	29.8	21.5	16.7	0.90	0.69	0.73	0.89
	SVR	11.5	36.7	21.6	20.9	0.89	0.67	0.77	0.85
	BPNN	22.5	61.6	22.1	25.9	0.54	0.22	0.82	0.78
	CNN	9.4	39.3	21.0	17.7	0.84	0.67	0.80	0.90
	RNN	**7.5**	27.2	25.5	14.5	**0.91**	0.74	0.78	0.91
	LSTM	9.3	**20.1**	**15.3**	**11.1**	0.90	**0.85**	**0.93**	**0.95**
Hawaii	ARIMA	14.4	38.7	15.4	12.5	0.80	0.53	0.76	0.77
	SVR	17.7	32.8	19.4	15.3	0.77	0.54	0.76	0.78
	BPNN	32.0	59.7	23.8	29.9	0.57	0.37	0.43	0.54
	CNN	12.2	32.1	7.3	11.1	0.83	0.54	0.92	0.70
	RNN	10.5	24.9	7.5	9.8	0.88	0.66	0.92	0.81
	LSTM	**5.9**	**18.1**	**6.2**	**8.2**	**0.95**	**0.86**	**0.95**	**0.91**

TABLE 7. Mape of daily forecast per month.

Location	Model	MAPE%											
		Jan.	Feb.	Mar.	Apr.	May	Jun.	Jul.	Aug.	Sep.	Oct	Nov.	Dec.
Atlanta	ARIMA	15.6	11.3	12.4	10.4	10.5	5.8	9.2	9.8	11.7	11.0	8.9	17.6
	SVR	18.6	15.6	15.5	12.3	14.7	11.9	8.0	12.1	12.3	15.0	10.4	20.2
	BPNN	26.9	24.6	20.5	18.2	10.2	12.6	12.2	14.9	12.5	18.5	22.9	41.2
	CNN	15.4	10.9	11.2	9.8	11.6	10.1	12.7	14.6	**8.0**	11.4	9.2	21.3
	RNN	11.3	11.6	7.8	**7.9**	7.8	7.9	7.1	7.0	8.9	10.5	9.5	15.9
	LSTM	**10.6**	**10.6**	**7.8**	8.2	**7.7**	**5.1**	**6.0**	**5.9**	9.5	**10.3**	**8.2**	**13.4**
New York	ARIMA	28.2	30.7	**15.8**	13.0	13.2	12.2	11.6	11.6	12.7	22.6	33.7	28.3
	SVR	35.9	35.4	23.0	17.1	14.1	16.4	15.3	12.9	11.3	28.0	40.4	25.1
	BPNN	33.2	37.5	33.5	28.4	17.3	20.5	13.5	18.1	23.8	22.2	54.9	20.3
	CNN	27.8	24.8	18.8	13.4	10.2	15.8	12.7	12.0	11.5	21.9	22.9	25.7
	RNN	26.0	26.5	21.5	10.7	14.9	12.6	9.7	10.7	12.5	24.0	36.0	23.6
	LSTM	**20.3**	**20.3**	18.5	**9.6**	**7.8**	**7.9**	**8.1**	**7.4**	**10.4**	**19.3**	**22.7**	**19.6**
Hawaii	ARIMA	9.5	9.5	10.8	10.0	15.3	13.2	13.3	12.4	14.7	13.4	19.9	13.7
	SVR	13.2	12.6	12.8	11.5	20.9	18.8	17.5	15.4	15.6	16.4	14.1	16.6
	BPNN	21.5	19.4	35.5	35.9	31.7	40.9	30.3	36.6	30.1	22.6	22.6	32.3
	CNN	6.8	8.1	10.2	11.1	11.2	14.7	13.2	14.3	11.3	10.5	11.3	13.7
	RNN	6.7	7.9	9.8	9.5	**9.5**	9.2	9.5	12.1	10.4	10.2	11.0	11.6
	LSTM	**3.2**	**3.5**	**5.9**	**9.4**	10.4	**7.5**	**7.3**	**9.3**	**10.2**	**6.1**	**10.3**	**10.3**

VI. CONCLUSION

The distributed photovoltaic system has the characteristics of intermittent, random and volatility, which is reflected in the distribution of solar irradiance in different seasons and weathers. Yu *et al.* [26] demonstrated in previous work that RNN has better prediction performance than BPNN and RBFNN in sunny, rainy and cloudy days. LSTM, as the deep structure of RNN, is a solution for vanishing gradient and exploding gradient caused due to its special hidden layer cell structure design, which allowed the RNN models with

LSTM units to model both short and long term temporal dependencies in time-series data. This study established a short-term prediction model based on LSTM to verify its potential to predict solar irradiance. In order to ensure the safe operation of the grid and improve the economics of the PV system, the timescale encompasses the amount of GHI one hour in advance and one day in advance. Samples used for forecasts were subdivided into spring, summer, fall, and winter, and the forecast results of sunny and cloudy as well as mixed days in different seasons, were investigated. In comparison with ARIMA, SVR and NN models, LSTM has a strong competitive advantage, especially on cloudy days and mixed days.

In areas with large latitude differences, their solar irradiance distribution and climate are significantly different. To verify the stability of LSTM, this study collected meteorological data from Atlanta, New York, and Hawaii, and further explored the scalability of LSTM. LSTM has demonstrated excellent forecasting performance for hourly forecasts on all weather, where the RMSE in Atlanta and New York is 45.84 W/m^2 and 41.37 W/m^2. Especially on mixed days, The RMSE of LSTM in Hawaii is 86.68 W/m^2, when the RMSE of BPNN, CNN, and RNN are 178.44 W/m^2, 195.92 W/m^2 and 183.29 W/m^2. From the results of daily forecast, LSTM's ability to predict on days with low solar irradiance is reduced, mainly in cloudy days. The MAPE of the LSTM model in Atlanta, New York, and Hawaii on cloudy days is 14.9%, 20.1%, and 18.1%. All R^2 on cloudy days is about 0.85. From Fig. 9, the high value of R^2 in Atlanta and New York is concentrated between April and September, referring to Fig. 3, which is exactly when the daily GHI value is high. LSTM still needs to improve predictive performance when GHI is low. However, the LSTM is still very effective in improving the prediction accuracy of RNN and has better prediction accuracy than other predictive models. On mixed days, RNN's MAPE in New York is up to 25.5%, while LSTM's MAPE is 15.3%, which is 10.2% better than RNN. On all days, LSTM's MAPE is the lowest, which is 8.0%, 11.1%, 8.2% in Atlanta, New York, and Hawaii.

REFERENCES

[1] S. Jiang, C. Wan, and C. Chen, "Distributed photovoltaic generation in the electricity market: Status, mode and strategy," *CSEE J. Power Energy Syst.*, vol. 4, no. 3, pp. 263–272, , Sep. 2018. doi: 10.17775/CSEEJPES.2018.00600.

[2] D. Millstein, R. Wiser, M. Bolinger, and G. Barbose, "The climate and air-quality benefits of wind and solar power in the United States," *Nature Energy*, vol. 6, no. 9, Aug. 2017, Art. no. 17134. doi: 10.1038/nenergy.2017.134.

[3] P. Hanser, "The practicality of distributed PV-battery systems to reduce household grid reliance," *Utilities Policy*, vol. 46, pp. 22–32, Jan. 2017. doi: 10.1016/j.jup.2017.03.004.

[4] P. Ramsami and V. Oree, "A hybrid method for forecasting the energy output of photovoltaic systems," *Energy Conversion Manage.*, vol. 95, pp. 406–413, May 2015. doi: 10.1016/j.enconman.2015.02.052.

[5] J. Olauson, M. N. Ayob, M. Bergkvist, N. Carpman, V. Castellucci, A. Goude, D. Lingfors, R. Waters, and J. Widén, "Net load variability in Nordic countries with a highly or fully renewable power system," *Nature Energy*, vol. 1, no. 12, Nov. 2016, Art. no. 16175. doi: 10.1038/nenergy.2016.175.

[6] A. Fentis, L. Bahatti, M. Tabaa, and M. Mestari, "Short-term nonlinear autoregressive photovoltaic power forecasting using statistical learning approaches and *in-situ* observations," *Int. J. Eng. Sci*, vol. 10, no. 10, pp. 189–206, Jun. 2019. doi: 10.1007/s40095-018-0293-5.

[7] F. Creutzig, P. Agoston, J. C. Goldschmidt, G. Luderer, G. Nemet, and R. C. Pietzcker, "The underestimated potential of solar energy to mitigate climate change," *Nature Energy*, vol. 2, no. 9, Aug. 2017, Art. no. 17140. doi: 10.1038/nenergy.2017.140.

[8] D. M. Kammen and D. A. Sunter, "City-integrated renewable energy for urban sustainability," *Science*, vol. 352, no. 6288, pp. 922–928, May 2016. doi: 10.1126/science.aad9302.

[9] J. Antonanzas, N. Osorio, R. Escobar, R. Urraca, F. J. Martinez-de-Pison, and F. Antonanzas-Torres, "Review of photovoltaic power forecasting," *Sol. Energy*, vol. 136, pp. 78–111, Oct. 2016. doi: 10.1016/j.solener.2016.06.069.

[10] H. Zhou, Y. Zhang, L. Yang, Q. Liu, K. Yan, and Y. Du, "Short-term photovoltaic power forecasting based on long short term memory neural network and attention mechanism," *IEEE Access*, vol. 7, pp. 78063–78074, 2019. doi: 10.1109/ACCESS.2019.2923006.

[11] G. Wang, Y. Su, and L. Shu, "One-day-ahead daily power forecasting of photovoltaic systems based on partial functional linear regression models," *Renew. Energy*, vol. 96, pp. 469–478, Oct. 2016. doi: 10.1016/j.renene.2016.04.089.

[12] M.-C. Kang, J.-M. Sohn, J.-Y. Park, S.-K. Lee, and Y.-T. Yoon, "Development of algorithm for day ahead PV generation forecasting using data mining method," in *Proc. MWSCAS*, Seoul, South Korea, 2011, pp. 1–4.

[13] V. Kushwaha and N. M. Pindoriya, "Very short-term solar PV generation forecast using SARIMA model: A case study," in *Proc. ICPS*, Pune, India, 2017, pp. 430–435.

[14] H. Lu and G. Chang, "Enhanced grey theory system model with weight table for now-casting PV power generation forecast," in *Proc. ISGT Asia*, Singapore, 2018, pp. 952–956.

[15] Y. Kashyap, A. Bansal, and A. K. Sao, "Solar radiation forecasting with multiple parameters neural networks," *Renew. Sustain. Energy Rev.*, vol. 49, pp. 825–835, Sep. 2015. doi: 10.1016/j.rser.2015.04.077.

[16] S. Alessandrini, L. D. Monache, S. Sperati, and G. Cervone, "An analog ensemble for short-term probabilistic solar power forecast," *Appl. Energy*, vol. 157, pp. 95–110, Nov. 2015. doi: 10.1016/j.apenergy.2015.08.011.

[17] H. Hasan, M. R. Munawar, and R. H. Siregar, "Neural network-based solar irradiance forecast for peak load management of grid-connected microgrid with photovoltaic distributed generation," in *Proc. ICELTICs*, Banda Aceh, Indonesia, 2017, pp. 87–90.

[18] G. Reikard, S. E. Haupt, and T. Jensen, "Forecasting ground-level irradiance over short horizons: Time series, meteorological, and time-varying parameter models," *Renew. Energy*, vol. 112, pp. 474–485, Nov. 2017. doi: 10.1016/j.renene.2017.05.019.

[19] L. Benali, G. Notton, A. Fouilloy, C. Voyant, and R. Dizene, "Solar radiation forecasting using artificial neural network and random forest methods: Application to normal beam, horizontal diffuse and global components," *Renew. Energ*, vol. 132, pp. 871–884, Mar. 2018. doi: 10.1016/j.renene.2018.08.044.

[20] R. De Leone, M. Pietrini, and A. Giovannelli, "Photovoltaic energy production forecast using support vector regression," *Neural Comput. Appl.*, vol. 26, no. 8, pp. 1955–1962, Nov. 2015. doi: 10.1007/s00521-015-1842-y.

[21] M. Reichstein, G. Camps-Valls, B. Stevens, M. Jung, J. Denzler, and N. Carvalhais, "Deep learning and process understanding for data-driven earth system science," *Nature*, vol. 566, no. 7743, pp. 195–204, Feb. 2019. doi: 10.1038/s41586-019-0912-1.

[22] S. Leva, A. Dolara, F. Grimaccia, M. Mussetta, and E. Ogliari, "Analysis and validation of 24 hours ahead neural network forecasting of photovoltaic output power," *Math. Comput. Simul.*, vol. 131, pp. 88–100, Jan. 2015. doi: 10.1016/j.matcom.2015.05.010.

[23] S. P. Durrani, S. Balluff, L. Wurzer, and S. Krauter, "Photovoltaic yield prediction using an irradiance forecast model based on multiple neural networks," *J. Mod. Power Syst. Clean Energy*, vol. 6, no. 2, pp. 255–267, Mar. 2018. doi: 10.1007/s40565-018-0393-5.

[24] A. Alfadda, S. Rahman, and M. Pipattanasomporn, "Solar irradiance forecast using aerosols measurements: A data driven approach," *Sol. Energy*, vol. 170, pp. 924–939, Aug. 2018. doi: 10.1016/j.solener.2018.05.089.

[25] Y. Sun, V. Venugopal, and A. R. Brandt, "Convolutional neural network for short-term solar panel output prediction," in *Proc. WCPEC*, Waikoloa Village, HI, USA, 2018, pp. 2357–2361.

[26] Y. Yu, J. Cao, X. Wan, F. Zeng, J. Xin, and Q. Ji, "Comparison of short-term solar irradiance forecasting methods when weather conditions are complicated," *J. Renew. Sustain. Energy*, vol. 10, no. 5, Sep. 2018, Art. no. 053501. doi: 10.1063/1.5041905.
[27] A. Rahman, V. Srikumar, and A. D. Smith, "Predicting electricity consumption for commercial and residential buildings using deep recurrent neural networks," *Appl. Energy*, vol. 211, pp. 372–385, Feb. 2018. doi: 10.1016/j.apenergy.2017.12.051.
[28] P.-J. Tang, H.-L. Wang, and K.-S. Xu, "Multi-objective layer-wise optimization and multi-level probability fusion for image description generation using LSTM," *Acta Automatica Sinica*, vol. 40, no. 7, pp. 1237–1249, Jul. 2018. doi: 10.16383/j.aas.2017.c160733.
[29] J. Li, A. Mohamed, G. Zweig, and Y. Gong, "LSTM time and frequency recurrence for automatic speech recognition," in *Proc. ASRU*, Scottsdale, AZ, USA, 2015, pp. 187–191.
[30] M. Romera, P. Talatchian, S. Tsunegi, F. A. Araujo, V. Cros, P. Bortolotti, J. Trastoy, K. Yakushiji, A. Fukushima, H. Kubota, S. Yuasa, M. Ernoult, D. Vodenicarevic, T. Hirtzlin, N. Locatelli, D. Querlioz, and J. Grollier, "Vowel recognition with four coupled spin-torque nano-oscillators," *Nature*, vol. 536, no. 7730, pp. 230–234, Nov. 2018. doi: 10.1038/s41586-018-0632-y.
[31] P. Tang, H. Wang, and S. Kwong, "Deep sequential fusion LSTM network for image description," *Neurocomputing*, vol. 312, pp. 154–164, 2018.
[32] G. Rao, W. Huang, Z. Feng, and Q. Cong, "LSTM with sentence representations for document-level sentiment classification," *Neurocomputing*, vol. 308, pp. 49–57, Sep. 2018.
[33] J. Zhou, Y. Lu, H.-N. Dai, H. Wang, and H. Xiao, "Sentiment analysis of chinese microblog based on stacked bidirectional LSTM," *IEEE Access*, vol. 7, pp. 38856–38866, 2019. doi: 10.1109/ACCESS.2019.2905048.
[34] L. Yang, Y. Zheng, X. Cai, H. Dai, D. Mu, and L. Guo, "A LSTM based model for personalized context-aware citation recommendation," *IEEE Access*, vol. 6, pp. 59618–59627, 2018. doi: 10.1109/ACCESS.2018.2872730.
[35] Y. Wang, D. Gan, M. Sun, N. Zhang, Z. Lu, and C. Kang, "Probabilistic individual load forecasting using pinball loss guided LSTM," *Appl. Energy*, vol. 235, pp. 10–20, Feb. 2019. doi: 10.1016/j.apenergy.2018.10.078.
[36] L. Peng, S. Liu, R. Liu, and L. Wang, "Effective long short-term memory with differential evolution algorithm for electricity price prediction," *Energy*, vol. 162, pp. 1301–1314, Nov. 2018. doi: 10.1016/j.energy.2018.05.052.
[37] J. Bedi and D. Toshniwal, "Deep learning framework to forecast electricity demand," *Appl. Energy*, vol. 238, pp. 1312–1326, Mar. 2019. doi: 10.1016/j.apenergy.2019.01.113.
[38] S. Muzaffar and A. Afshari, "Short-term load forecasts using LSTM networks," *Energy Procedia*, vol. 158, pp. 2922–2927, Feb. 2019. doi: 10.1016/j.egypro.2019.01.952.
[39] Y. Huang, L. Shen, and H. Liu, "Grey relational analysis, principal component analysis and forecasting of carbon emissions based on long short-term memory in China," *J. Cleaner Prod.*, vol. 209, pp. 415–423, Feb. 2018. doi: 10.1016/j.jclepro.2018.10.128.
[40] Z. Cen and J. Wang, "Crude oil price prediction model with long short term memory deep learning based on prior knowledge data transfer," *Energy*, vol. 169, pp. 160–171, Feb. 2018. doi: 10.1016/j.energy.2018.12.016.
[41] A. Habte, M. Sengupta, and A. Lopez. (2017). *Evaluation of the National Solar radiation Database (NSRDB): 1998–2015*. Accessed: Apr. 2017. [Online]. Available: https://www.nrel.gov/docs/fy17osti/67722.pdf
[42] M. J. Reno and C. W. Hansen, "Identification of periods of clear sky irradiance in time series of GHI measurements," *Renew. Energy*, vol. 90, pp. 520–531, May 2016. doi: 10.1016/j.renene.2015.12.031.
[43] H. Liu, L. Li, Y. Han, and F. Lu, "Method of identifying the lengths of equivalent clear-sky periods in the time series of DNI measurements based on generalized atmospheric turbidity," *Renew. Energy*, vol. 136, pp. 179–192, Jun. 2019. doi: 10.1016/j.renene.2018.12.119.
[44] S. Wang and H. Chen, "A novel deep learning method for the classification of power quality disturbances using deep convolutional neural network," *Appl. Energy*, vol. 235, pp. 1126–1140, Feb. 2019. doi: 10.1016/j.apenergy.2018.09.160.
[45] T. Wang, R. G. Qiu, and M. Yu, "Predictive modeling of the progression of Alzheimer's disease with recurrent neural networks," *Sci. Rep.*, vol. 8, no. 1, Jun. 2018, Art. no. 9161. doi: 10.1038/s41598-018-27337-w.
[46] J. Lago, F. De Ridder, and B. De Schutter, "Forecasting spot electricity prices: Deep learning approaches and empirical comparison of traditional algorithms," *Appl. Energy*, vol. 221, pp. 386–405, Jul. 2018. doi: 10.1016/j.apenergy.2018.02.069.
[47] Y. LeCun, Y. Bengio, and G. Hinton, "Deep learning," *Nature*, vol. 521, pp. 436–444, May 2015. doi: 10.1038/nature14539.
[48] L. Palagi, A. Pesyridis, E. Sciubba, and L. Tocci, "Machine learning for the prediction of the dynamic behavior of a small scale ORC system," *Energy*, vol. 166, pp. 72–82, Oct. 2018. doi: 10.1016/j.energy.2018.10.059.
[49] F. Wang, Z. Zhen, Z. Mi, H. Sun, S. Su, and G. Yang, "Solar irradiance feature extraction and support vector machines based weather status pattern recognition model for short-term photovoltaic power forecasting," *Energy Buildings*, vol. 86, pp. 427–438, Jan. 2015. doi: 10.1016/j.enbuild.2014.10.002.

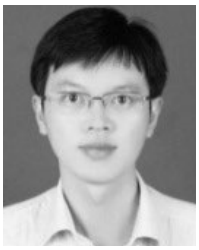

YUNJUN YU was born in Shangrao, China. He received the B.Sc. and M.Sc. degrees in control theory and control engineering from Nanchang University, China, in 2000 and 2007, respectively, and the Ph.D. degree from the Chinese Academy of Sciences, in 2013. He is currently an Associate Professor with the Department of Electrical and Automation Engineering, Information Engineering School, Nanchang University. His research interests include photovoltaic forecasting, fault diagnosis, data-driven optimal control and its applied in photovoltaic microgrid systems, ADRC, and low-carbon electricity technology.

JUNFEI CAO received the B.S. degree in automation from Nanchang University, Jiangxi, China, in 2016, where he is currently pursuing the M.S. degree in control engineering. His research interests include photovoltaic forecasting and acceleration of neural networks.

JIANYONG ZHU received the Ph.D. degree. He is currently an Associate Professor with East China Jiaotong University. His research interests include modeling and optimal control of complex industrial process, stochastic distribution control, predictive control, and intelligent control systems.